10-11-2023

Modulating poisson's ratio in flexible honeycombs by density and architecture gradations

Kazi Zahir Uddin

Ibnaj A. Anni

George Youssef

Behrad Koohbor

Modulating poisson's ratio in flexible honeycombs by density and architecture gradations

Engineering Research Express

PAPER

Modulating poisson's ratio in flexible honeycombs by density and architecture gradations

Kazi Zahir Uddin[1], **Ibnaj Anamika Anni**[1], **George Youssef**[2] **and Behrad Koohbor**[1,3,*]

[1] Department of Mechanical Engineering, Rowan University, 201 Mullica Hill Rd., Glassboro, NJ 08028, United States of America
[2] Experimental Mechanics Laboratory, Department of Mechanical Engineering, San Diego State University, 5500 Campanile Drive, San Diego, CA 92182, United States of America
[3] Advanced Materials and Manufacturing Institute, Rowan University, 201 Mullica Hill Rd., Glassboro, NJ 08028, United States of America
* Author to whom any correspondence should be addressed.

E-mail: koohbor@rowan.edu

Keywords: additive manufacturing, cellular solids, auxetic, density gradation, Poisson's ratio

OPEN ACCESS

RECEIVED
4 July 2023

REVISED
9 September 2023

ACCEPTED FOR PUBLICATION
26 September 2023

PUBLISHED
11 October 2023

Abstract

Zero Poisson's ratio structures are a new class of mechanical metamaterials wherein the absence of lateral deformations allows the structure to adapt and conform their geometries to desired shapes with minimal interventions. These structures have gained attention in large deformation applications where shape control is a key performance attribute, with examples including but not limited to shape morphing, soft robotics, and flexible electronics. The present study introduces an experimentally driven approach that leads to the design and development of (near) zero Poisson's ratio structures with considerable load-bearing capacities through concurrent density and architecture gradations in hybrid honeycombs created from hexagonal and re-entrant cells. The strain-dependent Poisson's ratios in hexagonal and re-entrant honeycombs with various cell wall thicknesses have been characterized experimentally. A mathematical approach is then proposed and utilized to create hybrid structures wherein the spatial distribution of different cell shapes and densities leads to the development of honeycombs with minimal lateral deformations under compressive strains as high as 0.7. Although not considered design criteria, the load-bearing and energy absorption capacities of the hybrid structures are shown to be comparable with those of uniform cell counterparts. Finally, the new hybrid structures indicate lesser degrees of instability (in the form of cell buckling and collapse) due to the self-constraining effects imposed internally by the adjacent cell rows in the structures.

1. Introduction

The demand for cost-effective manufacturing of materials with superior mechanical performance and adaptable functionalities has grown significantly in the past two decades. In particular, emerging areas of soft robotics, flexible electronics, and lightweight aeronautical structures have witnessed revolutionary innovations, only made possible by developing novel materials and structures with extraordinary characteristics not found in conventional material systems. An example of such structures is cellular polymers (including stochastic, e.g., foams, and ordered or lattice structures), wherein the geometry, connectivity, and architecture of cells in the structure play critical roles in determining their physical and mechanical performance attributes [1].

Auxetic cellular structures constitute a novel class of cellular solids, wherein the microarchitectural features can be adjusted to manifest unconventional negative Poisson's ratios (NPR) at macroscales [2, 3]. In addition to provoking scientific curiosity to explore the nature of such unusual and counter-intuitive behaviors, synthetic auxetic structures also show mechanical performance superior to those found in their non-auxetic counterparts [4]. For example, various auxetic structures reported concurrent improvements in stiffness, strength, fracture resistance, and mechanical energy absorption capacity [5–9]. A drawback associated with using auxetic structures, especially in large deformation applications (e.g., flexible electronics and soft robotics), is their strongly strain-dependent Poisson behavior. That is, the initial negative Poisson's ratios tend to vary

substantially during large deformation loading events, often starting at a negative value and approaching zero or even positive (non-auxetic) values at larger strains. Evidence for such strongly strain-dependent auxetic response has been reported for elastomeric foams and additively manufactured cellular structures [10–13], noting that an uncontrollable Poisson effect can adversely affect the performance and the sought application of the auxetic structures.

In addition to NPR structures, cellular solids with zero Poisson's ratio (ZPR) have also gained attention, especially in shape-morphing applications [14–16]. Strongly strain-dependent Poisson's ratios in ZPR structure can also impose limitations on the structural performance since shape morphing materials and structures are, by design, expected to undergo large deformations. A practical approach recently proposed to address the strain-dependent Poisson's ratio in auxetic (and non-auxetic) cellular structures is the spatial gradation of microstructural and architectural features along specific directions such that the structure, as a whole, retains its ZPR characteristics over an extended strain range [12, 17]. This approach has been presented and discussed in flexible planar structures and their thicker load-bearing counterparts fabricated using center-symmetric perforations [12, 18, 19]. The so-called perforation-graded designs enabled the fabrication of flexible sheets with near-zero Poisson's ratios over tensile strains ranging from zero to higher than 0.5 [12].

Following the recent developments in designing Poisson's ratio-modulated structures, the present work discusses a new approach, where the Poisson behavior in flexible load-bearing structures is spatially tailored by combining density and architecture gradients. Flexible honeycombs with hexagonal (non-auxetic) and re-entrant (auxetic) cell geometries with various cell wall thicknesses are additively fabricated using thermoplastic polyurethane (TPU). Mechanical properties and Poisson's ratios of the uniform density structures are characterized using full-field measurements. Revealed by full-field strain measurements, the Poisson's ratios in the uniform-density structures are indicated to be highly strain-dependent, showing highly negative (characteristic of low-density, re-entrant structures) to highly positive (typical of high-density hexagonal structures) values. A simple yet effective approach is then implemented to enable the design of density- and architecture-graded honeycomb structures with minimal strain-dependent Poisson's ratios. Emphasis has been placed on the design of near-zero Poisson's ratio structures with enhanced compressive strength and energy absorption characteristics.

2. Experimental

2.1. Materials and sample preparation

Honeycomb structures with hexagonal and re-entrant cells containing a 9×9 array of cells were manufactured using fused filament fabrication (FFF). As shown in figure 1, honeycombs with 77 cells were fabricated. The cell geometries considered herein incorporated four different wall thicknesses (t) of 0.5 mm, 1 mm, 1.5 mm, and 2 mm, corresponding to four different macroscopic densities [1]. Regardless of the wall thickness, each cell maintained a consistent internal arm length (l_1) of 2.31 mm and a width (l_2) of 6 mm. The overall in-plane height (h) varied across all samples due to the variations in wall thickness. All samples were additively manufactured using 100% in-fill with a Creality Ender 3 printer with a 0.4 mm nozzle diameter. Thermoplastic polyurethane (TPU) was selected as the base material for the structures due to its well-studied hyperelastic mechanical response, forming highly flexible load-bearing structures [20–22]. Figure 1(c) shows the magnified view of a single cell in a 3D-printed re-entrant honeycomb. The printing parameters used to fabricate all samples in this work (i.e., print speed, nozzle, and print bed temperature) were based on the optimized conditions identified and discussed in previous publications [12, 20, 21].

2.2. Mechanical testing

Honeycomb structures were subjected to uniaxial quasi-static in-plane compressive loads (-y direction) applied at a constant displacement rate of 5 mm.min^{-1}. Loading was stopped when the samples were compressed to 80% of their original height. A five-megapixel camera was used to capture images from the deforming samples during mechanical tests. The images captured during the deformation were later processed in the digital image correlation (DIC) software Vic-2D (Correlated Solutions, Inc., SC, USA) to determine the distribution of in-plane strain components. To improve image contrast and enable the DIC analysis, the front surface of the samples was coated with a matte black-and-white speckle pattern applied using spray paints. Due to the large deformation conditions in this work, the speckle pattern was applied just before each test to ensure the damp paint had enough ductility to deform with the sample. Although the speckle-patterned wall thicknesses allowed for the study of cell wall deformation (similar to those reported in [23, 24]), the scope of the present study only required macroscale deformation measurements. As such, the black-and-white nature of the cell structure (improved by placing a blackout blanket behind the samples during testing) was deemed sufficient for macroscopic strain measurements. Figure 2 shows a typical sample before the mechanical tests start, also

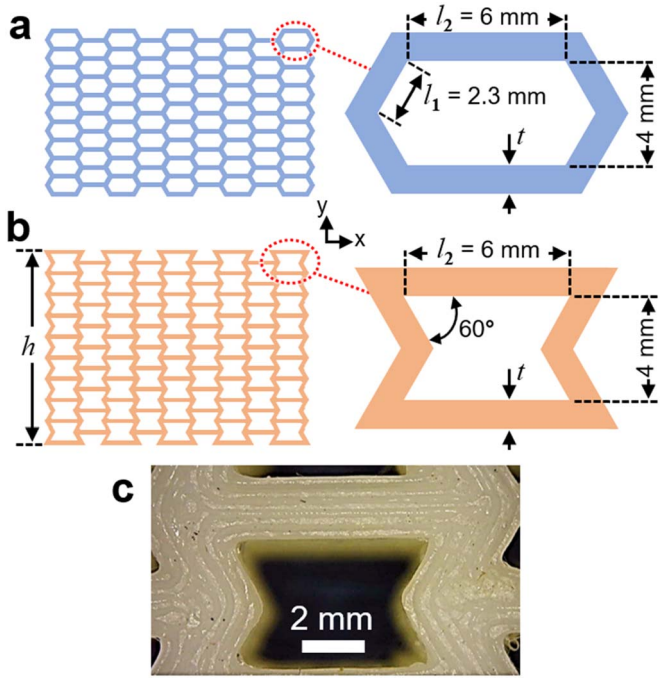

Figure 1. Schematic view of the 9×9 cell structures with the close-up view of a representative cell shown on the right for (a) hexagonal and (b) re-entrant honeycombs. Except for the wall thickness, *t*, all geometric features were maintained constant in all honeycombs. All internal angles in hexagonal honeycombs were 120°. (c) Material flow lines in a single re-entrant cell after 3D printing.

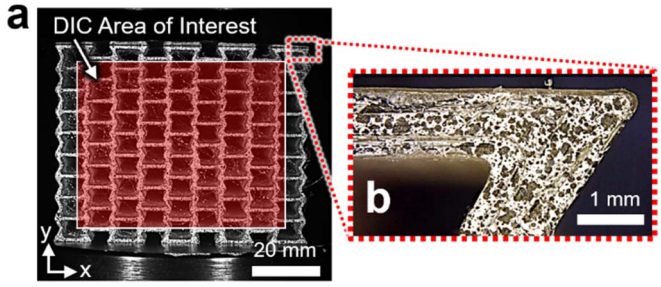

Figure 2. (a) A re-entrant structure showing the macroscopic DIC area of interest and the optical strain gauges used for the measurement of axial, ε_{yy}, and transverse, ε_{xx}, strain components. (b) a typical speckle pattern applied on the sample surface.

illustrating the macroscale DIC area of interest and the speckle-patterned cell walls. Note that while not necessary, the presence of a DIC-suitable pattern helps the image correlation algorithm with more effective subset tracking.

The in-plane normal strain components determined from image correlation were used to extract the macroscopic Poisson's ratio in each structure. Due to the highly heterogeneous deformation patterns in honeycomb structures (especially in re-entrant honeycombs), macroscopic Poisson's ratio is often calculated as the average of several single-point measurements [25]. In the present study, macroscale Poisson's ratio for the hexagonal and re-entrant honeycombs was calculated as the ratio between the transverse, ε_{xx}, and axial, ε_{yy}, strains (i.e., $\upsilon = -\varepsilon_{xx}/\varepsilon_{yy}$) averaged over the entire area of interest, as shown in figure 2. Previous reports on hyperelastic cellular solids (including foams) have proven the effectiveness of spatial averaging as a practical approach in investigating macroscale Poisson behavior [26].

The compressive engineering stress–strain curves obtained from the mechanical tests were also reported for the honeycomb structures. The stress values were calculated as the ratio of the applied compressive force and the sample surface in contact with the compression platens. Engineering (global) strain was calculated as the change of height normalized by the initial sample height. The strain energy absorption capacity of the samples was evaluated based on the efficiency, η, metric, defined as the ratio between the specific energy and the stress, expressed as,

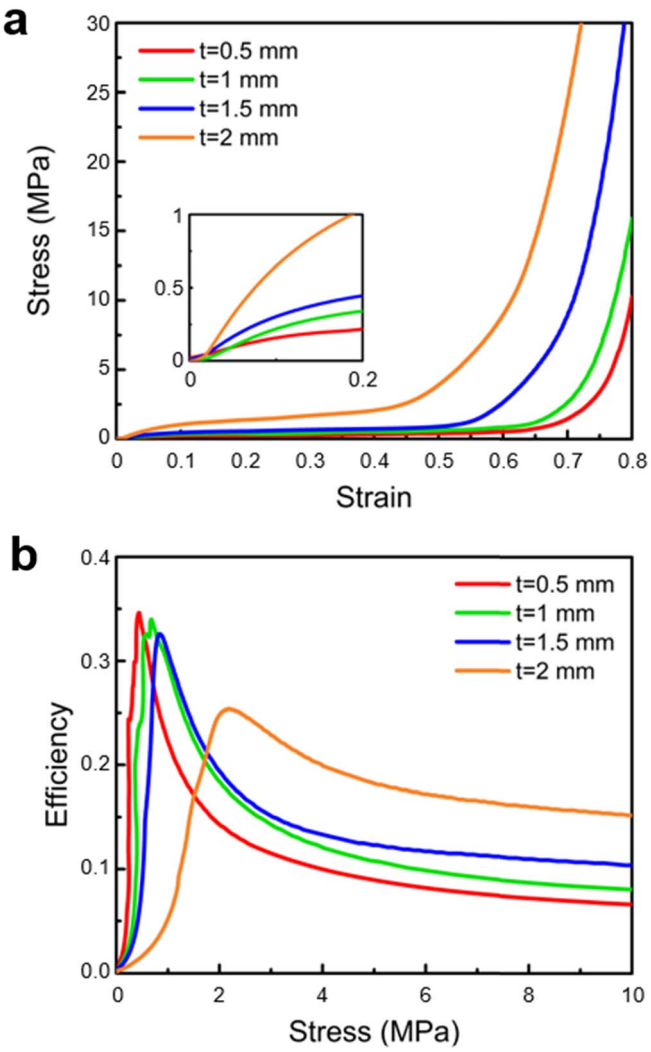

Figure 3. (a) Stress–strain, and (b) efficiency-stress curves obtained for hexagonal honeycombs with various wall thicknesses.

$$\eta = \frac{\int_0^{\varepsilon} \sigma(\varepsilon) d\varepsilon}{\sigma} \tag{1}$$

where, σ and ε represent global engineering stress and strain, respectively.

3. Results and discussion

3.1. Stress–strain response

Figure 3(a) shows the stress–strain curves for hexagonal honeycombs as a function of the wall thicknesses ranging from 0.5 to 2 mm. All curves are represented by an initial linear region, indicative of linear elastic deformation, followed by a stress plateau. The transition from linear to stress plateau is associated with cell wall instability, causing the vertical cell walls to buckle [1]. The strain range associated with the stress plateau strongly depends on the cell wall thickness. Thicker cell walls lead to enhanced strength (i.e., higher plateau levels) at the expense of the plateau span.

The stress plateau transitions into the densification stage, represented by a rapid increase in the slope of the stress–strain curve. The critical point at which this transition takes place (referred to as the densification onset) can be quantified by the maximum of the efficiency curve (see equation (1)). As shown in figure 3(b), the energy absorption efficiency is highest for the 0.5 mm wall thickness honeycomb; however, at significantly lower stress levels for this structure compared with others. On the other hand, while the maximum energy absorption efficiency for the 2 mm structure is the lowest amongst the hexagonal honeycomb structures considered here, it peaks at significantly higher stress levels. Hence, the potential promise of the thicker honeycombs as better energy absorbers in applications that require improved strength and energy absorption simultaneously.

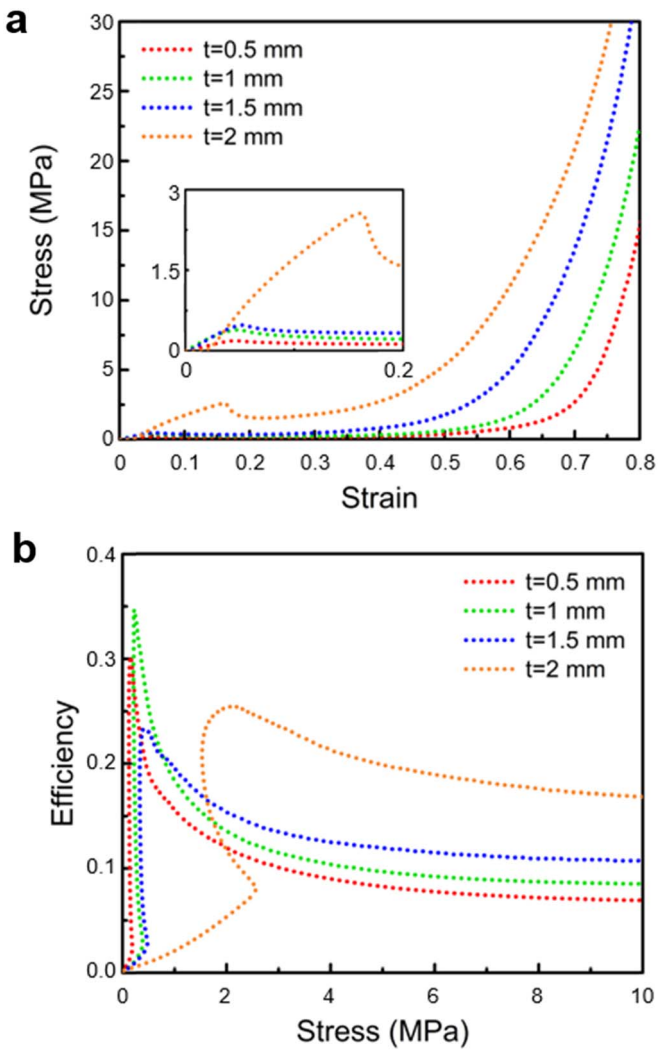

Figure 4. (a) Stress–strain, and (b) efficiency-stress curves obtained for re-entrant honeycombs with various wall thicknesses.

Similar to the hexagonal honeycombs, the stress–strain and efficiency curves were also obtained for the re-entrant structures. Figure 4(a) shows the stress–strain responses of the re-entrant honeycombs with various cell wall thicknesses. The stress–strain responses also signify an initial linear region, a stress plateau, and a final densification stage. However, the main differences between these curves and those of the hexagonal honeycombs are (1) a significant drop in stress at the transition between linear and plateau regions and (2) a comparably narrower plateau span. The initial drop in stress is associated with the instability mechanisms governed by the inward deformation patterns in the re-entrant honeycombs. As the applied compressive stress increases, the hourglass-shaped cells in the honeycomb buckle inward, causing early instability and a temporary decrease in stress. The latter occurs as the buckling instability implies a sudden loss of stiffness while the structure deforms due to the stored energy before buckling. As such, the solid cell walls undergo expedited instability, causing premature collapse, collectively shown by the stress drop in the stress–strain curve before the plateau. The stress plateau is then initiated and persists as the strain increases, eventually reaching the densification phase, similar to what was observed in the hexagonal honeycombs.

As shown in figure 4(b), the energy absorption efficiency response of the re-entrant structures is strongly affected by the stress drop at the onset of the plateau. Unlike the hexagonal honeycombs, the maximum energy absorption efficiencies of re-entrant structures show a nonmonotonic correlation with wall thickness. The efficiency parameter drops from its highest value for wall thicknesses of 1 mm, 0.5 mm, 2 mm, and 1.5 mm, respectively. In addition, the densification onset in re-entrant honeycombs (represented by maximum efficiency) occurs at relatively lower stresses than the hexagonal counterparts. As discussed in the forthcoming section, the investigated honeycomb structures exhibit distinct differences in the wall thickness-dependent deformation and instability mechanisms. The latter mechanisms also contributed to the irregular behaviors observed for the energy absorption performance of the re-entrant structures.

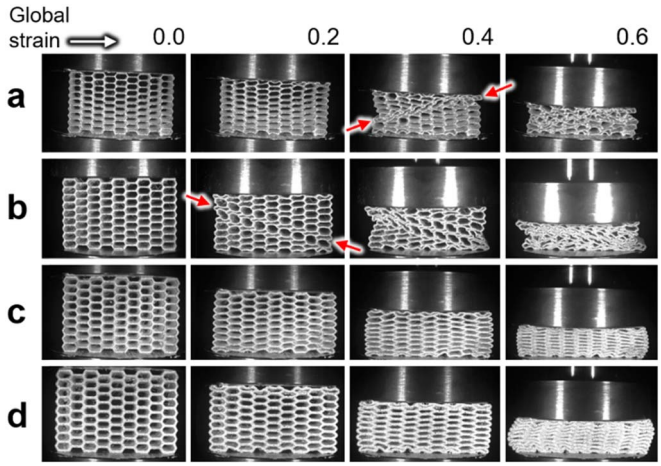

Figure 5. Deformation of hexagonal honeycombs at various global strains for samples with wall thicknesses of (a) 0.5 mm, (b) 1 mm, (c) 1.5 mm, and (d) 2 mm. Shear bands developed in thinner structures are marked by red arrows.

3.2. Deformation mechanisms and instability

Deformation responses of all honeycombs in this work were monitored by *in situ* imaging and DIC analyses. Figure 5 shows the sequential deformation configurations of hexagonal honeycombs with various cell wall thicknesses at different global strains. The two thinner wall honeycombs, i.e., with $t = 0.5$ and 1 mm, exhibit macroscale shear band formation at global compressive strains as low as 0.2, corresponding to the early stages of the stress plateau shown in figure 3. At these global strain magnitudes, the cell walls bend and buckle from the highest stress location, at the contact area between the compression platens and the structures. The locally buckled cell walls propagate diagonally throughout the structure, forming the discussed macroscale shear band. The progressive development of the cell wall collapse and shear bending across the entire height of the structure occurs at nearly constant stress levels, giving rise to the stress plateaus discussed earlier.

Similar bending-dominated instability occurs at hexagonal honeycombs with $t = 1$ mm. However, the increase in load-carrying solid sections within the thicker structures further resists bending and buckling deformations, leading to a belated shear band formation. In addition, the higher buckling resistance of the thicker cell walls leads to sequential deformation patterns due to the more even distribution of local stresses in the structure. As such, the structure shows more solid-like behavior with less densification and larger outward lateral expansions under compression (indicative of higher Poisson's ratios, as discussed later). This trend is more pronounced in the thickest cell wall structure, showing the largest lateral expansion and highest Poisson's ratio among all hexagonal honeycombs examined here.

Similar image-based qualitative deformation assessments were made for the re-entrant structures, as shown in figure 6. A C-shape macroscale buckling was observed in all re-entrant honeycombs tested here, irrespective of the cell wall thickness. This behavior stems from inward-facing corners in these structures that are geometrically constrained and forced to buckle inward from one side and outward from the other, causing an asymmetric deformation pattern. Such an early instability mode triggers a temporary relief from the applied compressive load, causing a drop in the stress–strain curve, as was discussed previously in figure 4(a). As the compressive load increases, the collapsed cell walls come into contact, causing densification and a second increase in the stress–strain curve. A noteworthy remark in the deformation of re-entrant structures is the consistent occurrence of the C-chape instability in all structures regardless of their cell wall thickness. As shown in figure 5, different parts of the re-entrant honeycombs slide over one another in a direction perpendicular to the load trajectory, thereby causing a shearing effect. This shearing effect leads to a highly heterogeneous strain distribution in the structure, challenging the development of structures with controllable lateral deformation. The latter concept justifies the significance of architectural gradation as a practical approach for Poisson's ratio modulation, as discussed in the following.

3.3. Full-field stain distribution and poisson's ratio

Images acquired during the mechanical tests were used to extract the distribution of in-plane strain fields in the structures. Figure 7 shows the distribution of in-plane axial strain, ε_{yy}, at a global strain of 0.4 in all honeycombs examined in this work. Consistent with the results and discussions presented in section 3.2., the degree of strain heterogeneity is shown to be highly dependent on the wall thickness in hexagonal honeycombs. The macroscale shear bands in the two thinner cell wall honeycombs (i.e., $t = 0.5$ and 1 mm) lead to considerable deformation

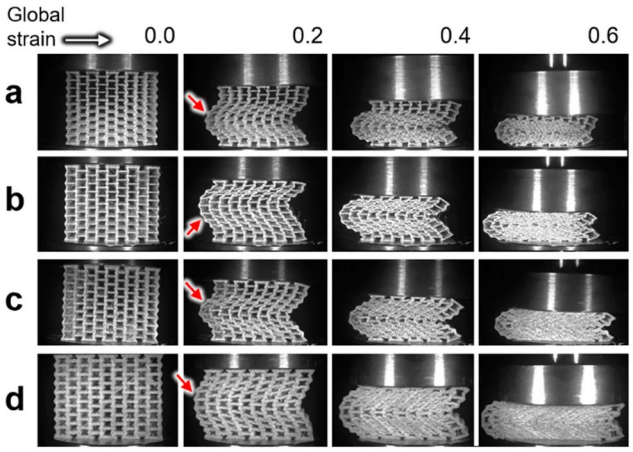

Figure 6. Deformation of re-entrant honeycombs at various global strains for samples with wall thicknesses of (a) 0.5 mm, (b) 1 mm, (c) 1.5 mm, and (d) 2 mm. Arrows point to the C-shaped instability in the structures.

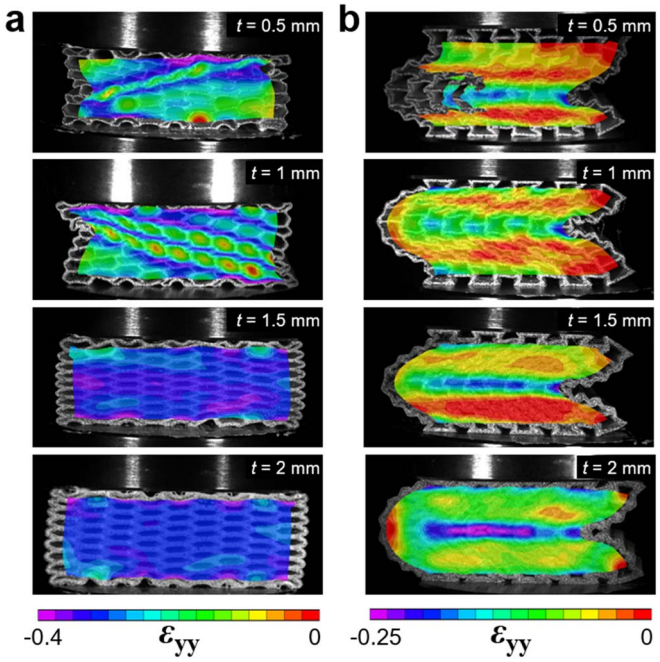

Figure 7. Distribution of in-plane axial strain fields, ε_{yy}, at a global strain of 0.4 in (a) hexagonal, and (b) re-entrant honeycombs with different wall thicknesses. The incomplete contour map in the re-entrant structure with $t = 0.5$ mm is due to the software limitations in subset tracking at large deformations conditions.

nonuniformities in the structures. In contrast, the two thicker cell wall hexagonal honeycombs show more uniform strain maps across the entire surface, mirroring the uniform deformations generated within each of the unit cells, making the structure (apodictic from the cell deformation underneath the superimposed contour maps). The full-field strain maps in the re-entrant structures exemplify the C-shape instability in the form of highly compressed horizontal bands located at the center of the structure, surrounded by relatively lower strain regions.

The highly heterogeneous strain patterns measured in the examined structures challenge the assessment of their Poisson's behavior, especially in cases where deformation patterns are asymmetric, i.e., the re-entrant structures. Therefore, the apparent (macroscale) Poisson's ratios were evaluated by calculating the in-plane strain fields averaged over the entire DIC area of interest in each sample. The strain-dependent Poisson's ratios are plotted in figure 8. Irrespective of the cell wall thickness, Poisson's ratios in the hexagonal structures show an initial positive value in the range of 0.3–0.4. The Poisson's behaviors of the two thicker cell wall hexagonal

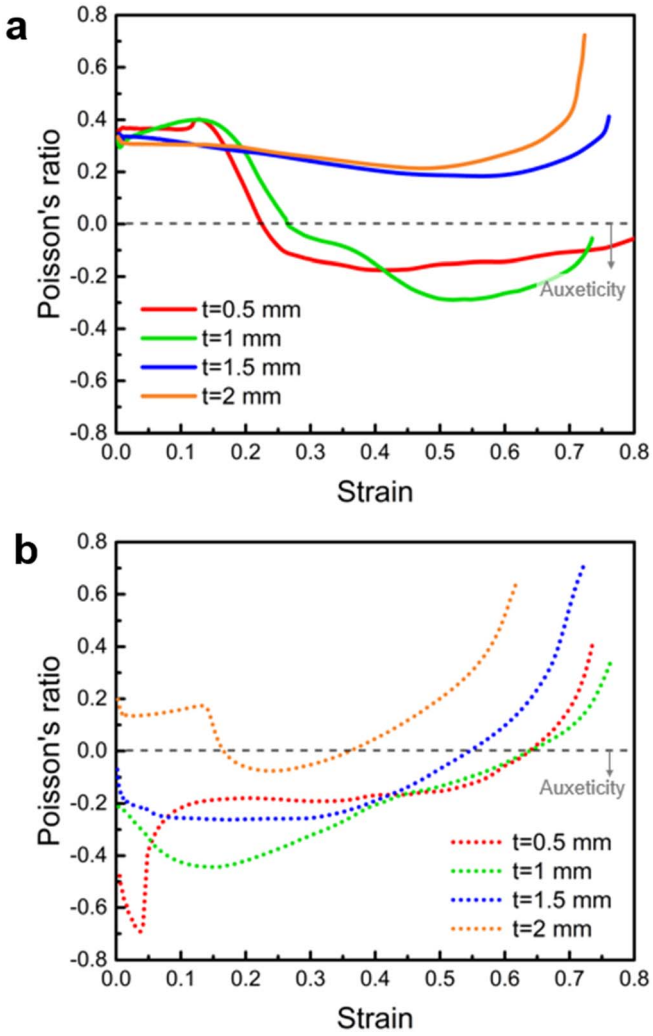

Figure 8. Variation of apparent Poisson's ratio with global strain for (a) hexagonal and (b) re-entrant structures with different wall thicknesses.

honeycombs (i.e., $t = 1.5$ and 2 mm) demonstrate a modest decrease over a strain range of 0–0.5. Upon reaching the densification onset, the Poisson's ratios increase rapidly, indicating the saturation of the axial deformation, after which the structure will only be capable of sustaining lateral deformation. In contrast, the two thinner cell wall hexagonal honeycombs show highly strain-dependent Poisson's ratios with nearly constant values up to 0.15 global strains, followed by a steep decrease to negative values at strains greater than 0.2. The steep drop and the counterintuitive pseudo-auxetic response in the thin hexagonal honeycombs relate to cell wall instability, causing the structure to collapse into itself, thereby limiting the outward lateral deformations. The latter two hexagonal honeycombs maintain their negative Poisson's behavior at larger compressive strains while showing an increasing trajectory.

Unlike hexagonal honeycombs, the re-entrant structures generally show smoother Poisson's behaviors, except for two step-wise changes in the thinnest and the thickest cell wall honeycombs due to the initiation of cell wall instability. The three thinner cell wall re-entrant honeycombs show negative Poisson's ratios (typical of and expected from re-entrant lattices [25]) with variable levels of strain dependence. Nonetheless, these structures retain their auxeticity up to global strains greater than 0.5. In contrast, at the onset of compression tests, Poisson's ratio of the thickest cell wall re-entrant structure resembles the non-auxetic behavior of the base material. This behavior is likely due to the presence of thick cell walls that resist buckling. This buckling-resistant behavior was also manifested in the stress–strain response of the same structure at strains below 0.13 (see figure 4(a)). Immediately after the initiation of the buckling at ~0.13 strain, the structure undergoes a rapid inward-facing lateral deformation that leads to a drop in the Poisson's ratio to negative values. Further increase of strain/stress leads to progressive structure densification, shown by a monotonic increasing trend in the Poisson's ratio. As such, the thickest cell wall re-entrant honeycomb only shows slight auxeticity over a strain range of 0.16–0.36, followed by an increase in values representative of a non-auxetic structure.

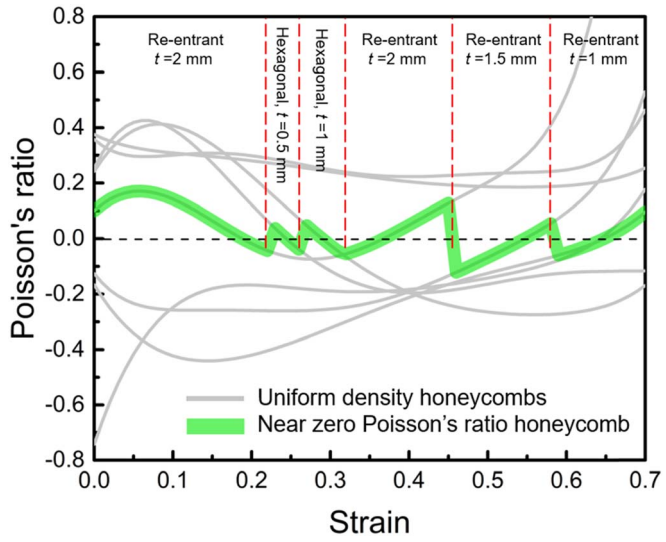

Figure 9. Identification of the geometric features (cell shape and wall thickness) that possess Poisson's ratios closest to zero at each strain level.

The Poisson's ratio data in figure 8 highlight two important findings about the examined structures. First, regardless of the cell architecture and density, Poisson's behavior in hyperelastic cellular lattices, like the ones examined herein, is highly strain dependent. Such strong strain dependence governs the auxetic versus non-auxetic behavior of the structure, leading to unconventional and uncontrollable deformation patterns. Second, developing zero Poisson's ratio structures (and structures with a strain-independent Poisson's behavior) may not be achieved using uniform cell structures. Instead, strain-independent Poisson's ratios for large strain applications may only be possible through the careful and rational combination of various cell shapes and thicknesses in graded structure. These remarks establish a practical approach that enables the design and development of honeycombs with near zero Poisson's ratios, discussed in the following.

3.4. Near zero poisson's ratio structures

Recent studies have indicated that Poisson's ratio-modulated structures can be developed by tailoring the deformation patterns through the spatial placement of architectural features (e.g., perforations and slits in planar structures) [19]. Investigations by the authors also suggest that Poisson's ratio modulations can facilitate the design of zero (or near zero) Poisson's ratio structures in flexible planar structures subjected to tensile loads. Similar concepts were implemented here to develop architecture- and density-graded structures that incorporate hexagonal and re-entrant structures with certain cell wall densities into a single hybrid honeycomb. The proposed approach is based on a simple optimization process that identifies the structures that exhibit near zero Poisson's ratios over certain strain ranges. The approach is visually illustrated in figure 9, wherein the near-zero Poisson's ratio structures corresponding to specific strain ranges are identified first. The identification process herein is based on a comparative algorithm that outputs the structural features (cell shape and cell wall thickness) that lead to Poisson's ratios closest to zero at a given strain value (i.e., min $|\upsilon^i(\varepsilon)|$ for ε:[0–0.7], where i represents the uniform density structures considered here, thus, $I = 8$). An alternative neural networks-based approach for the optimization of local architecture with targeted deformation behaviors was recently proposed by Deng *et al* [27]. Such algorithms are constructed using large datasets that include cell architecture-property correlations for a variety of different morphologies, and thus, require large material libraries as input. For simplicity, the present approach only uses the datasets obtained here and does not include all possible cell shape-cell wall pairs in the design space. Therefore, it is reasonable to assume that the forecasted near-zero structures do not represent the truly optimized conditions and are not expected to show perfectly strain-independent Poisson behaviors. Nonetheless, the graded structures designed here possess certain architectural and density features that make them uniquely different from those with uniform cell shapes and cell wall thicknesses (i.e., mono-density structures).

The near-zero Poisson's ratio structure in this work was designed based on the volumetric gradients corresponding to different strain ranges. For example, considering the Poisson's ratio curves shown in figure 9, among all the honeycombs examined herein, the thickest cell wall ($t = 2$ mm) re-entrant structure is shown to offer a Poisson's ratio closest to zero over the 0–0.22 and 0.32–0.45 strain windows. Similarly, for the strain windows of 0.23–0.26 and 0.27–0.31, hexagonal honeycombs with $t = 0.5$ mm and $t = 1$ mm are identified as the

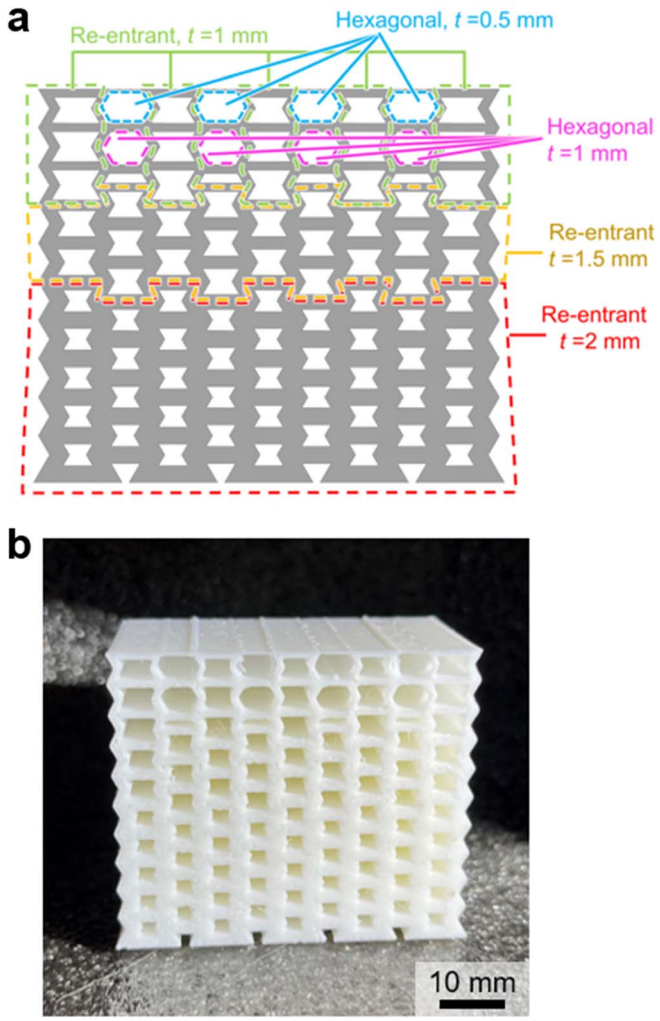

Figure 10. (a) Schematic view of the near ZPR honeycomb design showing various cell types and wall thicknesses at various locations. (b) Photograph of the as-printed hybrid structure.

nearest to ZPR structures, respectively. Finally, re-entrant cells with $t = 1.5$ mm and $t = 1$ mm are identified as the desired cell geometries for strain windows of 0.46–0.58 and 0.59–0.7, respectively.

The final step in designing near-zero Poisson's ratio structure is to determine the volume fraction (in terms of the number of cells) of the aforementioned cell features incorporated inside a hybrid honeycomb. This goal was achieved by determining the approximate volume fraction of the cells that correspond to the strain ratios described above. For example, of the 77 cells embedded in the hybrid honeycomb, 52% (corresponding to 0–0.22 and 0.32–0.45 normalized by 0.7 strain) must be re-entrant cells with $t = 2$ mm. Similarly, 18% and 17% of the 77 cells are designed as re-entrant cells with $t = 1.5$ mm and $t = 1$ mm wall thicknesses, respectively. Finally, hexagonal cells with $t = 1$ mm and $t = 0.5$ mm are to cover 7% and 6% of the total number of cells in the near-zero Poisson's ratio hybrid structure.

The hybrid (graded) structure with the above-mentioned geometric and density features was designed and additively manufactured for further evaluation. Figure 10 depicts the CAD drawing and the 3D printed near zero Poisson's ratio structure. This structure was subjected to a quasi-static compression testing scenario similar to what was used for the uniform-density honeycombs. *In situ* imaging and DIC analyses were also utilized to characterize the deformation response and macroscale Poisson's ratio of the hybrid structures. As shown by the grayscale images and their corresponding strain contour maps in figure 11, the deformation of the graded structure differs significantly from its constituents. The macroscale deformation response is shown to be significantly more homogeneous than the mono-density honeycombs (especially comparing the hybrid structure with re-entrant honeycombs). At the same time, the self-constraining effects [12] imposed on certain rows by their neighboring cells lead to an effective and favorable control of spatial instability and cell collapse in the structure. As such, the degree of instability, exhibited by the shear banding and C-shape buckling are limited in the hybrid honeycomb. Finally, as shown in figure 11(c), experimental measurements prove that the graded

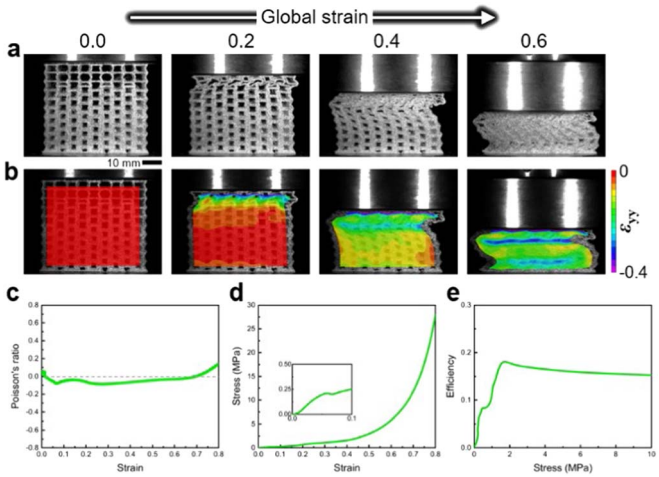

Figure 11. (a) Images showing the deformation response of the hybrid structure at various global strains, with the corresponding in-plane axial strain fields shown in (b). (c) Macroscale Poisson's ratio, (d) Stress–strain, and (e) Efficiency-stress curves of the hybrid near zero Poisson's ratio structure.

structure retains a near-zero Poisson's ratio over a significantly broad strain range while possessing mechanical characteristics comparable with the strongest and most energy-absorbing uniform honeycombs. The latter is evident when comparing the stress–strain (figure 11(d)) and efficiency-stress (figure 11(e)) behaviors of the hybrid structure with those of uniform-density honeycombs.

4. Conclusions

Local tailoring of density and cell architecture can be an effective approach in developing Poisson's ratio-modulated cellular structures. This concept was investigated in the present study by designing and creating near-zero Poisson's honeycomb structures from the hybridization of hexagonal and re-entrant honeycombs with various cell wall thicknesses. Several uniform-density hexagonal and re-entrant honeycombs were developed. Mechanical tests supplemented by image correlation analyses were conducted to characterize the macroscale Poisson's behavior of the structures. The strain-dependent Poisson's ratios of the uniform-density honeycombs were used as input to a simple mathematical approach that enabled the design of hybrid honeycombs whose Poisson's ratios remain near zero over broad strain spans. Results herein shed light on the significance of density and cell geometry gradations as two key parameters that enable designing Poisson's ratio-adjusted load-bearing structures for various applications.

Acknowledgments

This material is based upon work supported by the National Science Foundation under Grant No. 2035660 (B. K.) and Grant No. 2035663 (G.Y.). B.K. gratefully acknowledges the financial support provided by the Advanced Materials & Manufacturing Institute at Rowan University. The authors wish to acknowledge Marcus Perotti and Christopher Morehead at Rowan University for assisting with experimental measurements.

Data availability statement

All data that support the findings of this study are included within the article (and any supplementary files).

ORCID iDs

Behrad Koohbor https://orcid.org/0000-0002-5787-4644

References

[1] Gibson L J and Ashby M F *Cellular Solids: Structures and Properties, 2nd edn.1997* (Cambridge University Press)
[2] Jiang W, Ren X, Wang S L, Zhang X G, Zhang X Y, Luo C *et al* 2022 Manufacturing, characteristics and applications of auxetic foams: a state-of-the-art review *Composites Part* B **235** 109733

[3] Duedek K K, Martinez J A I, Ulliac G and Kadiac M 2022 Micro-scale auxetic hierarchical mechanical metamaterials for shape morphing *Adv. Mater.* **34** 2110115
[4] Grima-Cornish J N, Cauchi R, Attard D, Gatt R and Grima J N 2020 Smart Honeycomb 'Mechanical Metamaterials' with Tunable Poisson's Ratios *Phys. Status Solidi* **257** 1900707
[5] Hu H and Zulifqar A 2016 *Auxetic Textile Materials - A review. Journal of Textile Engineering & Fashion Technology* **1** 00002
[6] Sahariah B J, Namdeo A and Khanikar P 2022 Composite-inspired multilattice metamaterial structure: an auxetic lattice design with improved strength and energy absorption *Materials Today Communications* **30** 103159
[7] Ren X, Das R, Tran P, Ngo T D and Xie Y M 2018 Auxetic metamaterials and structures: a review *Smart Mater. Struct.* **27** 023001
[8] Joseph A, Mahesh V and Harursammpath D 2021 On the application of additive manufacturing methods for auxetic structures: a review *Advances in Manufacturing* **9** 342–68
[9] Vyavahar S and Jumar. S 2020 Re-entrant auxetic structures fabricated by fused deposition modeling: an experimental study of influence of process parameters under compressive loading *Polym. Eng. Sci.* **60** 3183–96
[10] Youssef G, Kokash Y, Uddin K Z and Koohbor B 2023 Density-dependent impact resilience and auxeticity of elastomeric polyurea foams *Adv. Eng. Mater.* **25** 2200578
[11] Koumlis S and Lmaberson. L 2019 Strain rate dependent compressive response of open cell polyurethane foam *Exp. Mech.* **59** 1087–103
[12] Pagliocca N, Uddin K Z, Anni I A, Shen C, Youssef G and Koohbor B 2022 Flexible planar metamaterials with tunable Poisson's ratios. *Mater. Des.* **215** 110446
[13] Uddin K Z, Pagliocca N, Anni I A, Youssef G and Koohbor B 2023 Multiscale strain field characterization in flexible planar auxetic metamaterials with rotating squares *Adv. Eng. Mater.* **25** 2201248
[14] Gaal V, Rodrigues V, Dantas S O, Galvao D S and Fonseca A F 2020 New zero poisson's ratio structures *Phys. Status Solidi* **14** 1900564
[15] Gong X, Huang J, Scarpa F, Liu Y and Leng J 2015 Zero poisson's ratio cellular structure for two-dimensional morphing applications *Compos. Struct.* **134** 384–92
[16] Gong X, Ren C, Sun J, Zhang P, Du L and Xie F 2022 3D zero poisson's ratio honeycomb structure for morphing wing applications *Biomimetics* **7** 198
[17] Rahman O, Uddin K Z, Muthulingam J, Youssef G, Shen C and Koohbor B 2022 Density-graded cellular solids: mechanics, fabrication *and applications* **24** 2100646
[18] Yao J, Sun R, Scarpa F, Remillat C, Gao Y and Su Y 2021 Two-dimensional graded metamaterials with auxetic rectangular perforations *Compos. Struct.* **261** 113313
[19] Yao J, Su Y, Scarpa F and Li Y 2022 An optimization approach to design deformation patterns in perforated mechanical metamaterials using distributions of Poisson's ratio-based unit cells *Compos. Struct.* **281** 115015
[20] Rahman O and Koohbor B 2020 Optimization of energy absorption performance of polymer honeycombs by density gradation *Composites Part C* **3** 100052
[21] Anni I A, Uddin K Z, Pagliocca N, Singh N, Rahman O, Youssef G and Koohbor B 2022 Out-of-plane load-bearing and mechanical energy absorption properties of flexible density-graded TPU honeycombs *Composites Part C* **8** 100284
[22] Bates S R G, Farrow I R and Trask R S 2019 Compressive behaviour of 3D printed thermoplastic polyurethane honeycombs with graded densities *Mater. Des.* **162** 130–42
[23] Pagliocca N, Youssef G and Koohbor B 2022 In-plane mechanical and failure responses of honeycombs with syntactic foam cell walls *Compos. Struct.* **295** 115866
[24] Singh A, Ngo V, Huynh N U, Koohbor B and Youssef G *Structural Performance of Glass Beads Reinforced Honeycomb Structures: Strain Rate, Cell Geometry, and Weight Ratio Effects (under review)*
[25] Luo H C, Ren X, Zhang Y, Zhang X Y, Zhang X G, Luo C, Cheng X and Xie Y M 2022 Mechanical properties of foam-filled hexagonal and re-entrant honeycombs under uniaxial compression *Compos. Struct.* **280** 114922
[26] Koohbor B, Pagliocca N and Youssef G 2021 A multiscale experimental approach to characterize micro-to-macro transition length scale in polymer foams *Mech. Mater.* **161** 104006
[27] Deng B, Zareei A, Ding X, Weaver J C, Rycroft C H and Bertoldi K 2022 Inverse design of mechanical metamaterials with target nonlinear response via a neural accelerated evolution strategy *Adv. Mater.* **34** 2206238